

Wave functions for quantum Monte Carlo calculations in solids: Orbitals from density functional theory with hybrid exchange-correlation functionals

Jindřich Kolorenč,^{1,2,*} Shuming Hu,¹ and Lubos Mitás¹

¹*Department of Physics and Center for High Performance Simulation,
North Carolina State University, Raleigh, North Carolina 27695, USA*

²*I. Institut für Theoretische Physik, Universität Hamburg, Jungiusstraße 9, 20355 Hamburg, Germany*
(Dated: February 14, 2022)

We investigate how the fixed-node diffusion Monte Carlo energy of solids depends on single-particle orbitals used in Slater–Jastrow wave functions. We demonstrate that the dependence can be significant, in particular in the case of 3d transition-metal compounds, which we adopt as examples. We illustrate how exchange-correlation functionals with variable exact-exchange component can be exploited to reduce the fixed-node errors. On the basis of these results we argue that the fixed-node quantum Monte Carlo provides a variational approach for optimization of effective hamiltonians with parameters.

PACS numbers: 64.70.-p, 71.15.-m, 71.15.Nc, 71.20.-b

I. INTRODUCTION

Steady increase in supercomputer performance over the last three decades stimulates development of very accurate electronic structure methodologies that provide detailed understanding of ever larger and more complex systems. Diffusion Monte Carlo (DMC) method^{1,2} is one of the prime examples of these advanced many-body approaches. It uses a stochastic process to refine a given many-body wave function $|\Psi_T\rangle$ towards the actual ground-state solution $|\Psi_0\rangle$. The antisymmetry of the wave function with respect to fermionic degrees of freedom is usually maintained by imposing the so-called fixed-node condition. In practice it means that the nodal surface (the subset of configuration space where the many-body wave function vanishes) is restricted to be the same as in the initial guess $|\Psi_T\rangle$ throughout the entire stochastic simulation. The basic premise is that high accuracy is achieved even when relatively simple functional forms are employed for $|\Psi_T\rangle$.

The impact of the fixed-node approximation has been intensively studied in few-electron atoms and molecules as well as in homogeneous systems, where the performance of the DMC method with increasing accuracy of the trial wave function $|\Psi_T\rangle$ is relatively well mapped out.^{3–8} Applications to solids are not nearly as numerous, and hence the influence of the fixed-node condition in crystalline settings is much less examined. Evaluation of bulk properties necessarily involves extrapolation to the thermodynamic limit, which decreases the amount of computational resources available for exploration of rather subtle fixed-node errors. Consequently, only the simplest trial wave functions, having the Slater–Jastrow form, are typically employed. These wave functions have nodal surfaces defined by single-particle orbitals, and therefore they correspond to mean-field nodes. The subject of our study are the fixed-node errors associated with such trial functions when they are applied to simple transition-metal oxides in crystalline phases.

II. FIXED-NODE DIFFUSION MONTE CARLO

The fixed-node diffusion Monte Carlo method calculates expectation values of quantum-mechanical operators in the ground state (as well as in certain excited states) of a many-body hamiltonian \hat{H} . The DMC wave function is found by a projection

$$|\Psi_D\rangle = \lim_{\tau \rightarrow \infty} e^{-\tau \hat{H}} |\Psi_T\rangle \quad (1a)$$

that gradually increases the weight of the lowest energy eigenstate of \hat{H} relative to all other states contained in some initially guessed wave function $|\Psi_T\rangle$. Building on similarity between the Schrödinger and the diffusion equations, the projection is realized with the aid of a classical stochastic process. The outcome of this simulation is a set of $3N$ -dimensional samples $\{R_i\}$ distributed according to a probability distribution $\mathcal{P}(R) = \Psi_D(R)\Psi_T(R)/\langle\Psi_D|\Psi_T\rangle$. Here $R = (\mathbf{r}_1, \mathbf{r}_2, \dots, \mathbf{r}_N)$ denotes coordinates of all N electrons comprising the investigated quantum system. The hamiltonian \hat{H} is assumed to be spin independent, which prevents any spin-flip processes to occur in Eq. (1a), and hence the spins do not enter the simulations as dynamical variables. The probabilistic interpretation of $\mathcal{P}(R)$ is possible only if it is a positive quantity. In the case of fermions, the projection as written in Eq. (1a) does not fulfill this requirement, which must therefore be prescribed in the form of an additional condition

$$\Psi_D(R)\Psi_T(R) \geq 0. \quad (1b)$$

This step introduces the so-called fixed-node approximation, since the projection cannot reach the true ground state $|\Psi_0\rangle$ if the fermionic nodes of the trial wave function $|\Psi_T\rangle$ differ from (a priori unknown) nodes of the desired ground state. Our primary aim is to explore the impact of this fixed-node approximation for a particular functional form of the trial wave function.

The set of \mathcal{N} samples $\{R_i\}$ acquired as a result of a DMC simulation can be directly used to calculate the

so-called mixed estimates of the quantum-mechanical expectation values,

$$\begin{aligned} \frac{\langle \Psi_D | \hat{A} | \Psi_T \rangle}{\langle \Psi_D | \Psi_T \rangle} &= \int dR \left(\frac{\Psi_D(R) \Psi_T(R)}{\langle \Psi_D | \Psi_T \rangle} \right) \left(\frac{[\hat{A} \Psi_T](R)}{\Psi_T(R)} \right) \\ &= \frac{1}{N} \sum_{i=1}^N \frac{[\hat{A} \Psi_T](R_i)}{\Psi_T(R_i)} + \mathcal{O}(N^{-1/2}). \end{aligned} \quad (2)$$

If the operator \hat{A} commutes with the hamiltonian, the mixed estimate equals the desired quantum-mechanical expectation value, $\langle \Psi_D | \hat{A} | \Psi_T \rangle / \langle \Psi_D | \Psi_T \rangle = \langle \Psi_D | \hat{A} | \Psi_D \rangle / \langle \Psi_D | \Psi_D \rangle$. In general, however, there is an error proportional to the difference between $|\Psi_D\rangle$ and $|\Psi_T\rangle$ that can be reduced to the next order using the following extrapolation²

$$\begin{aligned} \frac{\langle \Psi_D | \hat{A} | \Psi_D \rangle}{\langle \Psi_D | \Psi_D \rangle} &= 2 \frac{\langle \Psi_D | \hat{A} | \Psi_T \rangle}{\langle \Psi_D | \Psi_T \rangle} - \frac{\langle \Psi_T | \hat{A} | \Psi_T \rangle}{\langle \Psi_T | \Psi_T \rangle} \\ &+ \mathcal{O}\left(\left| \frac{\Psi_D}{\sqrt{\langle \Psi_D | \Psi_D \rangle}} - \frac{\Psi_T}{\sqrt{\langle \Psi_T | \Psi_T \rangle}} \right|^2\right). \end{aligned} \quad (3)$$

The expectation value $\langle \Psi_T | \hat{A} | \Psi_T \rangle / \langle \Psi_T | \Psi_T \rangle$ is evaluated by straightforward Monte Carlo integration and it is referred to as the estimate of the variational Monte Carlo (VMC) method.

III. TRIAL WAVE FUNCTIONS

We employ trial wave functions having the Slater–Jastrow functional form, which is an antisymmetrized product of single-particle orbitals (Slater determinant) multiplied by a correlation factor that is symmetric with respect to pair-electron exchanges. We can write

$$\Psi_T(R) = \det\{\psi_\alpha^\uparrow\} \det\{\psi_\beta^\downarrow\} e^{J(R, X)}, \quad (4)$$

where ψ_α^\uparrow and ψ_β^\downarrow are spatial parts of single-particle orbitals that correspond to spin-up respectively spin-down electronic states. The vector $X = (\mathbf{x}_1, \mathbf{x}_2, \dots, \mathbf{x}_M)$ encompasses positions of all M ions in the lattice. The expression in Eq. (4) represents only a spatial component of the trial wave function corresponding to one particular spin configuration, where electrons with labels $1, \dots, N_\uparrow$ are in the spin-up state and electrons with labels $N_\uparrow + 1, \dots, N$ are in the spin-down state. We can use this simplified form with fixed spin states instead of the full wave function as long as neither the hamiltonian nor any other operator, expectation value of which we intend to calculate, depend on electron spins. The applications we consider involve only cases with zero total spin, i.e., N is an even number and $N_\uparrow = N_\downarrow = N/2$.

The Jastrow correlation factor we use,

$$J(R, X) = \sum_{i,j} f(\mathbf{r}_i - \mathbf{r}_j) + \sum_{i,I} g(\mathbf{r}_i - \mathbf{x}_I), \quad (5)$$

contains one- and two-body terms, g and f , that are parametrized in the same way as in Ref. 9. This correlation factor improves efficiency of the Monte Carlo sampling and accuracy of general expectation values calculated according to Eq. (3). Quality of the DMC total energy E_D depends solely on the accuracy of the nodal surface that is, given the functional form of Eq. (4), completely determined by the single-particle orbitals $\{\psi_\alpha^\uparrow, \psi_\beta^\downarrow\}$. Ideally, these orbitals would be parametrized by an expansion in a saturated basis with the expansion coefficients varied to minimize the DMC total energy. Unfortunately, the stochastic noise and the computational demands of the DMC method make this route extremely inefficient in practice except, perhaps, in the case of the simplest few electron systems.

A more feasible alternative is to skip the DMC projection, Eq. (1a), and optimize the orbitals $\{\psi_\alpha^\uparrow, \psi_\beta^\downarrow\}$ with respect to a simpler quantity than E_D . For instance, the variational Monte Carlo methodology can be employed to minimize the variational energy $E_V = \langle \Psi_T | \hat{H} | \Psi_T \rangle / \langle \Psi_T | \Psi_T \rangle$. The VMC optimization of one-particle orbitals was successfully employed for atoms and small molecules of the first-row atoms,^{6,10,11} but the method is still too demanding for applications to solids. It is also not completely robust, since an improvement of the variational energy does not automatically guarantee an improvement of the fixed-node energy due to the limited parametric freedom of the trial wave function $|\Psi_T\rangle$. This issue is even more pronounced when trial wave functions are not optimized with respect to the VMC energy, but with respect to another quantity, such as the energy variance.

To avoid the large number of variational parameters needed to describe the single-particle orbitals, another family of methods has been proposed. The orbitals in the Slater–Jastrow wave function are found as solutions to self-consistent-field (SCF) equations that represent a generalization of the Hartree–Fock equations.^{12,13} The correlations described by the Jastrow factor enter the SCF equations via variational Monte Carlo techniques. These methods were tested in atoms as well as in solids,^{12,14} albeit only rather limited variational freedom was allowed in the employed Jastrow factors. Unfortunately, wave functions derived in this way did not lead to lower DMC energies compared to wave functions with orbitals from the Hartree–Fock theory or from the local density approximation (LDA).^{12,15} It is unclear, whether the lack of observed improvements in the fermionic nodal surfaces stems from insufficient flexibility of the employed correlation factors or from too small set of tested cases, all with only s and p valence electrons.

In this paper we also use SCF equations as a means to construct the one-particle orbitals, but the parametric dependence of these equations is introduced without any relation to the actual Jastrow factor. The self-consistent-field equations in question are Kohn–Sham equations corresponding to the hybrid exchange-correlation functional

PBE0_w,¹⁶

$$E_{xc}^{PBE0_w} = wE_x^{HF} + (1-w)E_x^{PBE} + E_c^{PBE}. \quad (6)$$

Here E_x^{PBE} and E_c^{PBE} are exchange and correlation parts of the PBE form¹⁷ of the generalized gradient approximation (GGA), and E_x^{HF} is the exchange from the Hartree–Fock theory. The weight w is in the range $0 < w < 1$ and serves as a variational parameter with respect to which the fixed-node DMC energy is minimized.

In the transition-metal oxides we study it is understood that exchange in GGA is underestimated,¹⁸ whereas the “exact” exchange from the Hartree–Fock theory overestimates the real exchange mechanism as any screening effects are neglected.^{19,20} The hybrid density-functional theory (DFT) provides an interpolating scheme between these two extremes. There are numerous examples in the literature illustrating that reasonable agreement of its predictions and experimental observations can be achieved.^{21–24}

Arguably, the single parameter introduced to the one-particle orbitals represents only relatively constrained variational freedom compared to the approaches mentioned above.^{6,10,11} On the other hand, the simplicity of the parameter space allows for direct optimization of the fixed-node DMC total energy, which improves robustness compared to minimization within the VMC method. Initial applications of this strategy to molecules^{9,25} and in a more elementary form also to solids²⁶ were reported previously. In the following sections we perform the DMC optimization for two compounds, MnO and FeO, and systematically analyze the variational freedom available within this method in crystalline environments.

IV. THERMODYNAMIC LIMIT

Crystals in our simulations are represented by periodically repeated simulation cells of a finite size, in which the Coulomb interaction energy is evaluated with the aid of the Ewald formula.^{1,27} To calculate bulk quantities one has to perform an extrapolation to the thermodynamic limit (infinite crystal volume). Our main objective, however, is to compare energies obtained for different trial wave functions in a given simulation cell with *fixed* volume, and hence the size extrapolation seems redundant. Indeed, the leading-order term of the finite-size errors related to the long-range character of the Coulomb interaction is a function of the average charge density alone.^{28,29} Variation of single-particle orbitals does not change this quantity, and these finite-size errors are therefore mostly irrelevant for our wave function optimization, since they cancel out.

The Coulomb interaction is not the only cause of finite-size biases in calculations performed in finite simulation cells. There is another source of non-vanishing surface terms that appear even if no two-body interaction is present in the hamiltonian.³⁰ These can be brought to light as follows: the statement “periodically repeated

TABLE I: Exact-exchange weight w leading to minimal DMC total energies of several phases of MnO and FeO solids.

compound	phase	V (Å ³ /XO)	w
MnO	B1 AFM-II	21.7	0.30 ± 0.01
MnO	B8 AFM	21.7	0.33 ± 0.01
FeO	B1 AFM-II	20.4	0.25 ± 0.02
FeO	B1 AFM-II	17.3	0.217 ± 0.006
FeO	iB8 AFM	17.0	0.156 ± 0.003

simulation cells” used above refers to observable quantities and does not fully specify the boundary condition for the phase of the wave function. In the language of single-particle description of solids, different boundary conditions compatible with periodicity of observables correspond to simulations being done at different k points. Averaging over all k points from the first Brillouin zone removes the dependence of the computed quantities on the boundary conditions and in the case of non-interacting particles it is equivalent to performing the thermodynamic limit. For hamiltonians with particle-particle interactions this correspondence is not exact, but a very substantial reduction of finite-size errors is observed nevertheless.³⁰

Comparison of trial wave functions at a single k point is certainly a valid approach. On the other hand, variation of the exchange-correlation functional in the Kohn–Sham equations modifies the resulting band structure in a generally non-trivial k -dependent manner, see for instance Ref. 21 for illustration. As a result, the minimization of the total energy calculated at a single k point does not necessarily lead to the same optimal weight w as does the minimization of the k -averaged total energy. Since the latter is arguably a better approximation of the thermodynamic limit, which is what we are ultimately interested in, we work with the k -averaged quantities.

V. MnO AT AMBIENT CONDITIONS

We start our investigations with manganese monoxide at experimental equilibrium volume, $V = 21.7$ Å³/MnO. Calculations are performed for two lattice structures, both with antiferromagnetic (AFM) ordering of magnetic Mn atoms: B1 (symmetry group R $\bar{3}m$, the so-called AFM-II state) and B8 (symmetry group P $\bar{3}m1$). The former phase is the low-temperature ground state structure at atmospheric pressure and the latter is a phase stable at high pressures.³¹ Since all states investigated in this paper are antiferromagnetic, we will often leave out this attribute.

Data were collected in simulation cells containing 16 atoms (8 Mn and 8 O). Atomic cores were replaced by norm-conserving pseudopotentials within the so-called localization approximation.³² Helium core was excluded from oxygen atoms³³ and neon core from manganese

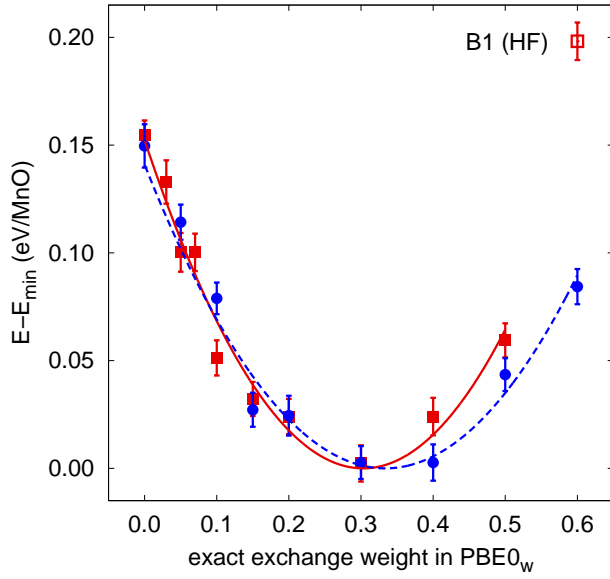


FIG. 1: (color online) The DMC total energy of MnO at experimental equilibrium volume ($V = 21.7 \text{ \AA}^3/\text{MnO}$) for two distinct structural phases: B1 AFM-II (red squares, solid line) and B8 AFM (blue points, dashed line). Minima of the fits are chosen as reference energies for the respective phases. Also shown is the DMC total energy of the B1 AFM-II phase obtained with the Hartree-Fock orbitals (empty red square).

atoms,³⁴ which left 168 valence and semi-core electrons explicitly included in the simulations.

The Monte Carlo simulations were performed with QWALK³⁵ and the single-particle orbitals were prepared in CRYSTAL2003.³⁶ In both codes, the orbitals were expanded in a gaussian basis, completeness of which was verified against a converged basis of linearized augmented plane waves as implemented in the WIEN2K code.³⁷ The basis set benchmarks were performed within DFT using the PBE-GGA exchange-correlation functional.

The acquired dependence of the DMC total energies on the exact-exchange weight w is plotted in Fig. 1. Each energy value shown in the picture represents an average over 8 k points. Such average made within DFT differs from the converged integral over the first Brillouin zone by less than the statistical error bars plotted in the figure. The quadratic functions fitted through the data using the least-squares method lead to the optimal values for the weight w listed in Tab. I. The behavior is virtually the same in both phases and the optimal weight is very close to the standard PBE0 choice¹⁶ $w = 0.25$. Drop of the total energy from the pure PBE-GGA orbitals ($\Leftrightarrow \text{PBE0}_{w=0}$) to the minimum is $\approx 0.15 \text{ eV/MnO}$, and from the Hartree-Fock orbitals ($\nrightarrow \text{PBE0}_{w=1}$) it is $\approx 0.2 \text{ eV/MnO}$. The dependence of the fixed-node DMC total energy on the admixture of the exact exchange is weaker in the MnO solid than in the MnO molecule, where the gain from the Hartree-Fock to hybrid DFT orbitals was observed as large as $\approx 0.6 \text{ eV}$.⁹ We attribute this differ-

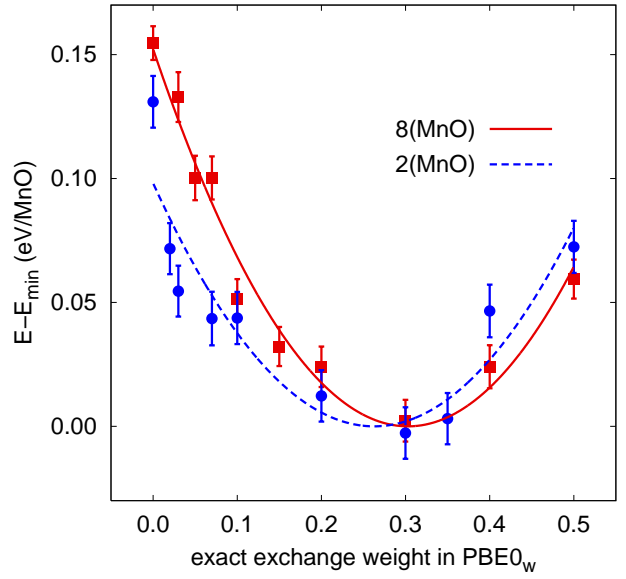


FIG. 2: (color online) The DMC total energy of MnO (B1 AFM-II phase at $V = 21.7 \text{ \AA}^3/\text{MnO}$) as a function of exact-exchange weight w . Compared are data obtained in simulation cells of two different sizes: 16 atoms (red squares, solid line) and 4 atoms (blue circles, dashed line). The lines are quadratic fits. Minima of these fits are chosen as reference energies for the respective data sets.

ence to a greater freedom of charge density to adapt in the molecule than in the constrained solid state environment.

The data collected so far can be utilized to evaluate quantities of direct physical interest. The difference between the optimized total energies provides a measure of relative stability of the investigated phases at the given volume. We find that the B1 structure is lower in energy than the B8 structure by $0.27 \pm 0.01 \text{ eV/MnO}$. The cohesive energy E_{coh} of MnO crystal can also be estimated. To this end, energies of isolated Mn and O atoms need to be calculated, and the crystalline total energy has to be extrapolated to the infinite volume. We provide details of these steps in Appendix A. In the end we obtain $E_{coh} = 9.29 \pm 0.04 \text{ eV}$ that is in good agreement with the value 9.5 eV derived from experimental formation enthalpies.³⁸ Our result differs from the earlier DMC estimate,^{39,40} which is not surprising as the present approach involves more advanced optimization of the trial wave function as well as much more thorough analysis of the finite-size errors.

VI. ARE LARGE SIMULATION CELLS NECESSARY?

It was argued in Sec. IV that k point averaging should remove nearly all finite-size biases relevant to the optimization of single-particle orbitals performed at a fixed

volume. It would certainly be beneficial if one could find the optimal exact-exchange weight in a small simulation cell and only then proceed with production runs in large cells.

We have repeated the optimization procedure in the primitive cell of the B1 AFM-II structure, which contains only 4 atoms (2 Mn and 2 O). All other parameters were kept unchanged, except the number of k points employed in the averaging had to be substantially increased—from 8 to 125—to achieve comparable convergence.⁴⁶ The necessity to enlarge the set of considered k points introduces an extra technical complication, since trial wave functions corresponding to the majority of these k points are complex-valued. Consequently, we replace the fixed-node DMC method with its natural generalization, the so-called fixed-phase DMC.⁴¹ The fixed-phase condition reduces to the fixed-node condition for real-valued trial wave functions.

The w -dependence of the DMC total energy calculated in the small simulation cell (Fig. 2) is similar but not completely identical to the behavior observed in the larger cell. The minimum is shifted to a slightly lower weight w and the $E(w)$ curve raises a little slower with w decreasing towards the pure PBE-GGA. It is plausible to assume that these differences are a fingerprint of the residual Coulomb finite-size effects.

VII. COMPRESSED FeO

Finally, we turn our attention to iron oxide subject to high pressures at low temperatures. We revisit our earlier study of the phase transition from the B1 AFM-II phase, stable at atmospheric pressure, to the iB8 AFM structure (space group $P6m2$), which the fixed-node DMC has predicted as stable above approximately 65 GPa.⁴² Calculations leading to this estimate used single-particle orbitals provided by the $\text{PBE0}_{w=0.2}$ functional. This choice was based on prior investigations^{9,25} and on a preliminary version of the results we present here. In the following, we analyze in detail how appropriate the $\text{PBE0}_{w=0.2}$ orbitals are in this case and how sensitive the transition pressure is to variations of single-particle orbitals in the Slater–Jastrow trial wave function.

We return back to simulation cells containing 16 atoms, partly because the orbital optimization appears more robust in larger cells (Sec. VI) and partly because we already acquired some data in the 16 atom cells in the course of our earlier investigations. The optimized values for the exact-exchange weight w in FeO are listed in Tab. I for experimental equilibrium volume $V = 20.4 \text{ \AA}^3/\text{FeO}$ as well as for two compressed states. The optimal proportion of the exact exchange decreases with compression, which is an expected phenomenon—the role of screening increases as the bands widen and a larger fraction of d electrons participates in chemical bonding.

In contrast to MnO, where B1 and B8 phases displayed very similar behavior, the two investigated structures of

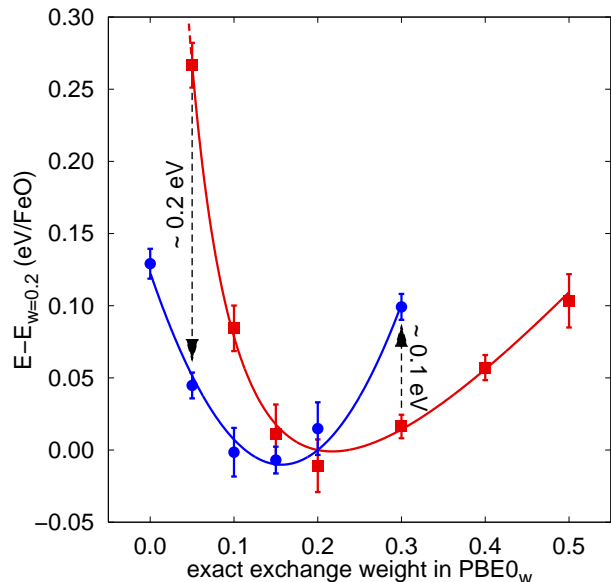


FIG. 3: (color online) The DMC total energy of compressed FeO in two phases: B1 AFM-II at $V = 17.3 \text{ \AA}^3/\text{FeO}$ (red squares), and iB8 AFM at $V = 17.0 \text{ \AA}^3/\text{FeO}$ (blue points). Lines are least square fits with a quadratic function in the iB8 phase, and with $E(w) = (a + bw + cw^2)/(d + w)$ in the B1 structure. Note the different choice of reference energies compared to Figs. 1 and 2. Here the zero energy for each phase is the value of the corresponding fit at $w = 0.2$.

FeO differ noticeably at comparable volumes. Detailed data for compressed FeO are shown in Fig. 3 to highlight the differences. Like in Sec. V, each total energy is obtained as an average over 8 k points. To facilitate comparison with our previous study,⁴² energies corresponding to the $\text{PBE0}_{w=0.2}$ orbitals are used as a reference. We can see that $w = 0.2$ indeed represents a reasonable compromise value, since corresponding DMC energies lie within error bars from the true minima.

In the case of the iB8 phase, the $E(w)$ data are well described by a quadratic function. In the B1 phase, on the other hand, the functional dependence is asymmetric around the minimum and a quadratic function does not provide a satisfactory fit. To locate the minimum for Tab. I, we used an alternative fitting function $E(w) = (a + bw + cw^2)/(d + w)$, which characterizes the calculated energies much better. Figure 3 shows that the energy raises rather fast when the exchange-correlation functional approaches the pure PBE-GGA. It does not come as a surprise, since the Kohn–Sham spectrum is metallic in the limit $w \rightarrow 0$, which is at odds with experimental facts. All other phases investigated here (FeO iB8 and both MnO phases) are insulating for all values of the weight w , and hence even orbitals close to the PBE-GGA provide reasonable trial wave functions.

The different behavior of the DMC total energies in the B1 and iB8 structures causes the pressure of the transition between these two phases to depend on the used

orbitals. To roughly estimate the variation of the transition pressure, we assume that the energy–volume equations of state of the respective phases only rigidly shift along the energy axis when the exchange weight is varied. The equations of state corresponding to the $\text{PBE0}_{w=0.2}$ orbitals were calculated in Ref. 42 and the corresponding shifts can be extracted from Fig. 3. When, for instance, the $\text{PBE0}_{w=0.3}$ orbitals are used, the iB8 phase is raised in energy by approximately 0.1 eV compared to the B1 structure, which leads to the transition pressure increased to ≈ 85 GPa. When the $\text{PBE0}_{w=0.05}$ orbitals are utilized, the iB8 phase is lowered by approximately 0.2 eV, which corresponds to the transition pressure of only ≈ 30 GPa. Evidently, the B1 to iB8 transition pressure is quite sensitive to the choice of the single-particle orbitals. Of course, the DMC method provides a definite prediction as long as the exchange weight is individually optimized in each phase. The pressure 65 ± 5 GPa derived in Ref. 42 remains valid as the actual DMC estimate for the B1 to iB8 transition pressure, since the energies obtained with the $\text{PBE0}_{w=0.2}$ orbitals lie within error bars from the minimal energies (Fig. 3).

VIII. OPTIMIZATION OF EFFECTIVE HAMILTONIANS

The optimization of not only the variational wave function but also of the effective hamiltonian can be considered in a broader context. The upper-bound property of the fixed-node approximation offers a new opportunity for finding optimal values of *any parameters* of effective hamiltonians in a consistent and well-defined manner. For example in DFT+ U methods,¹⁸ the Hubbard parameter U as well as the form of the double counting terms could be optimized in a similar way as the exact-exchange weight in the presented calculations. The optimized hamiltonian can subsequently be utilized for further calculations. We illustrate this on the density of states of the iron oxide shown as a function of the exact-exchange weight in Fig. 4. Note that for $\text{PBE0}_{w=0.2}$, i.e., for the functional that we used as optimal for the calculations of the equation of state, the single-particle spectrum exhibits a reasonable value of the gap of about 2.9 eV, which is much closer to the experimental value (≈ 2.4 eV, Ref. 43) than either pure GGA or pure Hartree–Fock limits. The key point is that although the hamiltonian was optimized in the ground state, the excitations are clearly improved as well.

In a more general sense, one could consider effective hamiltonians with more parameters and/or with more elaborated content beyond the one-particle form, such as explicit treatment of particle pairs, for example. The idea of employing the fixed-node DMC method could be of importance for such constructions as the most accurate and explicitly variational method available at present.

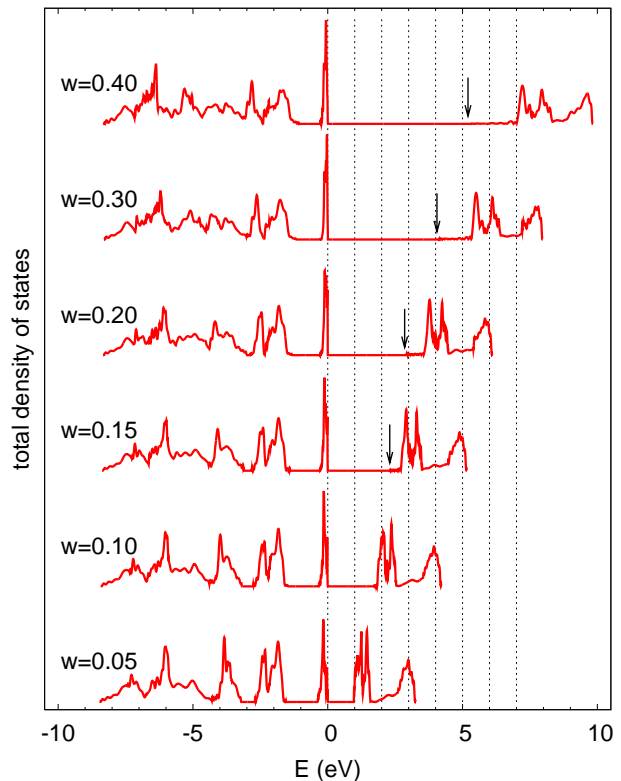


FIG. 4: (color online) Density of states of FeO (B1 phase at $V = 20.4 \text{ \AA}^3/\text{FeO}$) from PBE0_w calculations with varying w . Where it is not obvious, the bottom of the conduction band is indicated with an arrow.

IX. CONCLUSIONS

We have found that single-particle orbitals in Slater–Jastrow wave functions represent a non-trivial variational parameters for fermionic nodes in 3d transition-metal compounds. When these orbitals are generated with the aid of an exchange-correlation functional with variable admixture of the exact exchange, the corresponding fixed-node DMC energies differ by several tenths of eV per transition-metal atom. These variations can translate to substantial quantitative changes in the phase diagram as demonstrated in the case of iron oxide. Consequently, some form of orbital optimization should be performed in order to confidently predict relative stability of different crystal structures and the location of corresponding phase transitions.

The optimal amount of exact exchange providing minimal DMC energies depends on the particular compound and on the specific structural phase, but it is generally close to the value of 25% typically used within the hybrid density-functional theory.¹⁶ Our calculations provide yet another confirmation that the hybrid DFT indeed provides an improved picture of investigated compounds compared to more conventional functionals (LDA and GGA).

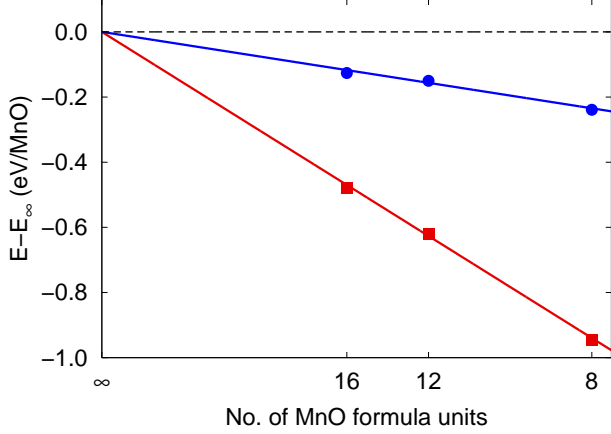


FIG. 5: (color online) Finite-size scaling for MnO (B1 AFM-II phase at $V = 21.7 \text{ \AA}^3/\text{MnO}$). All data points are averaged over 8 k points. Statistical error bars are smaller than symbol sizes. Red squares correspond to the Ewald formula for the Coulomb interaction energy, blue points include additional correction described in the text. Lines are least-squares fits with $E(N) = a/N + E_\infty$.

Acknowledgements

Support by NSF EAR-05301110, DMR-0804549 and OCI-0904794 grants and by DOE DE-FG05-08OR23336 Endstation grant is gratefully acknowledged. This study was enabled by INCITE and CNMS allocations at ORNL and by allocation at NCSA. J. K. would like to acknowledge financial support by the Alexander von Humboldt Foundation during preparation of the manuscript. We would like to thank M. Bajdich for numerous discussions on wave function optimization.

Appendix A: Cohesive energy of MnO

We have evaluated DMC energies of MnO crystal in three simulation cells containing 16, 24 and 32 atoms. The results obtained with the $\text{PBE0}_{w=0.3}$ orbitals are plotted in Fig. 5. Clearly, the averaging over 8 k points performed in all cases successfully suppresses differences in shapes of the individual simulation cells and the remaining size dependence can be very well fitted with a function $E(N) = a/N + E_\infty$. The estimate for E_∞ is -120.203 ± 0.001 hartree/MnO.

The a/N term can be substantially reduced by techniques described in Refs. 28 and 29. One part of the proposed correction to the Ewald total energy reads

$$\Delta E_{S(k)} = \frac{1}{4\pi^2} \int_D d^3k \frac{S(\mathbf{k})}{k^2}. \quad (\text{A1})$$

The static structure factor $S(\mathbf{k})$ entering the expression is defined as $S(\mathbf{k}) = \langle \Psi_0 | \hat{\rho}_{\mathbf{k}} \hat{\rho}_{-\mathbf{k}} | \Psi_0 \rangle / N$ with $\hat{\rho}_{\mathbf{k}}$ standing for a Fourier component of the electron density. The integral

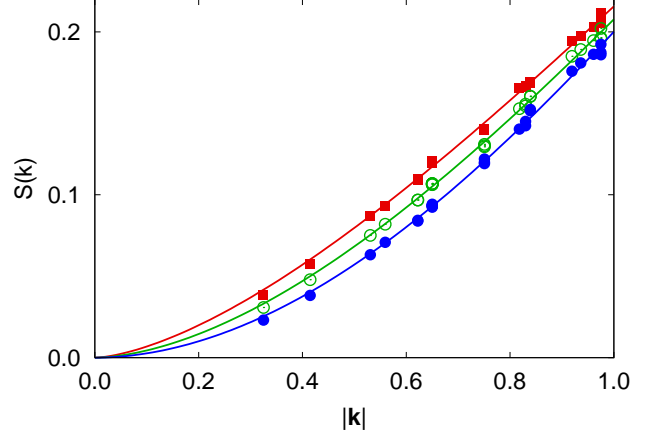


FIG. 6: (color online) Static structure factor $S(\mathbf{k})$ in MnO (B1 AFM-II phase at $V = 21.7 \text{ \AA}^3/\text{MnO}$). Calculations were performed with the $\text{PBE0}_{w=0.3}$ orbitals. Data are combined from simulation cells containing 16, 24 and 32 atoms. Plotted are: VMC estimate (red squares), mixed DMC estimate (green empty circles) and extrapolated DMC estimate (blue filled circles). The lines are fits with $S(k) = [1 - \exp(-\alpha k^\beta)]$.

in Eq. (A1) runs over a domain D centered around $\mathbf{k} = 0$ and having volume $8\pi^3/\Omega$, where Ω is volume of the simulation cell. The structure factor $S(\mathbf{k})$ is evaluated along the DMC simulation at a discrete set of points and then extrapolated towards $\mathbf{k} = 0$. We show this extrapolation for the present case in Fig. 6, where we compare mixed and extrapolated DMC estimates, Eqs. (2) and (3). The small- k behavior of $S(\mathbf{k})$ is found to be $\sim k^{1.7}$ for the mixed estimate and $\sim k^{1.9}$ for the extrapolated one. This variance originates in a limited quality of our trial wave functions at large distances between electrons—the Jastrow factor we use is restricted to zero for inter-electron separations larger than the Wigner–Seitz radius, and hence the correct long-range asymptotics cannot be fully captured. In the end, this deficiency is irrelevant, since the prediction of the extrapolated estimate is sufficiently close to the exact asymptotics $\sim k^2$ that translates to $\Delta E_{S(k)} \sim 1/N$.^{28,29} The total energies corrected according to Eq. (A1) are shown in Fig. 5 together with the pure Ewald data. The correction reduces the finite-size errors by 75%.

For calculations of individual atoms we utilize the same form of the trial wave function as we did in solids in order to stay within the same level of theoretical description.

TABLE II: Fixed-node DMC total energy of isolated Mn atom calculated using several sets of single-particle orbitals.

single-particle orbitals	E (hartree)
restricted open-shell HF	-104.0133 ± 0.0006
unrestricted HF	-104.0185 ± 0.0005
unrestricted $\text{PBE0}_{w=0.3}$	-104.0192 ± 0.0002

Single-particle orbitals for atomic calculations were obtained using GAMESS code.⁴⁴ Fixed-node DMC energies for the manganese atom corresponding to several choices of orbitals are listed in Tab. II. The difference between Hartree–Fock and PBE0_{w=0.3} is negligible for our purposes, since it is smaller than the statistical error bar

achieved for the energy of the bulk crystal.

Variation of single-particle orbitals in the trial wave function for the oxygen atom does not lead to any appreciable differences of DMC energies. To evaluate the cohesion of MnO, we use the result quoted in Ref. 45, $E_O = -15.8421 \pm 0.0002$ hartree.

-
- * On leave from Institute of Physics, Academy of Sciences of the Czech Republic, Na Slovance 2, CZ-18221 Praha 8, Czech Republic
- ¹ W. M. C. Foulkes, L. Mitas, R. J. Needs, and G. Rajagopal, *Rev. Mod. Phys.* **73**, 33 (2001).
 - ² B. L. Hammond, W. A. Lester, Jr., and P. J. Reynolds, *Monte Carlo Methods in Ab Initio Quantum Chemistry* (World Scientific, Singapore, 1994).
 - ³ M. Casula, C. Attaccalite, and S. Sorella, *J. Chem. Phys.* **121**, 7110 (2004).
 - ⁴ M. Bajdich, L. Mitas, G. Drobný, L. K. Wagner, and K. E. Schmidt, *Phys. Rev. Lett.* **96**, 130201 (2006).
 - ⁵ P. L. Ríos, A. Ma, N. D. Drummond, M. D. Towler, and R. J. Needs, *Phys. Rev. E* **74**, 066701 (2006).
 - ⁶ C. J. Umrigar, J. Toulouse, C. Filippi, S. Sorella, and R. G. Hennig, *Phys. Rev. Lett.* **98**, 110201 (2007).
 - ⁷ Y. Kwon, D. M. Ceperley, and R. M. Martin, *Phys. Rev. B* **58**, 6800 (1998).
 - ⁸ M. Holzmann, B. Bernu, and D. M. Ceperley, *Phys. Rev. B* **74**, 104510 (2006).
 - ⁹ L. K. Wagner and L. Mitas, *J. Chem. Phys.* **126**, 034105 (2007).
 - ¹⁰ C. Filippi and C. J. Umrigar, *J. Chem. Phys.* **105**, 213 (1996).
 - ¹¹ J. Toulouse and C. J. Umrigar, *J. Chem. Phys.* **128**, 174101 (2008).
 - ¹² C. Filippi and S. Fahy, *J. Chem. Phys.* **112**, 3523 (2000).
 - ¹³ N. Umezawa and S. Tsuneyuki, *J. Chem. Phys.* **119**, 10015 (2003).
 - ¹⁴ R. Sakuma and S. Tsuneyuki, *J. Phys. Soc. Jpn.* **75**, 103705 (2006).
 - ¹⁵ R. Prasad, N. Umezawa, D. Domin, R. Salomon-Ferrer, and W. A. Lester, Jr., *J. Chem. Phys.* **126**, 164109 (2007).
 - ¹⁶ J. P. Perdew, M. Ernzerhof, and K. Burke, *J. Chem. Phys.* **105**, 9982 (1996).
 - ¹⁷ J. P. Perdew, K. Burke, and M. Ernzerhof, *Phys. Rev. Lett.* **77**, 3865 (1996).
 - ¹⁸ V. I. Anisimov, J. Zaanen, and O. K. Andersen, *Phys. Rev. B* **44**, 943 (1991).
 - ¹⁹ M. D. Towler, N. L. Allan, N. M. Harrison, V. R. Saunders, W. C. Mackrodt, and E. Aprà, *Phys. Rev. B* **50**, 5041 (1994).
 - ²⁰ R. J. Needs and M. D. Towler, *Int. J. Mod. Phys. B* **17**, 5425 (2003).
 - ²¹ M. Alfredsson, G. D. Price, C. R. A. Catlow, S. C. Parker, R. Orlando, and J. P. Brodholt, *Phys. Rev. B* **70**, 165111 (2004).
 - ²² C. Franchini, V. Bayer, R. Podloucky, J. Paier, and G. Kresse, *Phys. Rev. B* **72**, 045132 (2005).
 - ²³ J. Kolorenč and L. Mitas, *Phys. Rev. B* **75**, 235118 (2007).
 - ²⁴ S. Kümmel and L. Kronik, *Rev. Mod. Phys.* **80**, 3 (2008).
 - ²⁵ L. Wagner and L. Mitas, *Chem. Phys. Lett.* **370**, 412 (2003).
 - ²⁶ E. Sola, J. P. Brodholt, and D. Alfè, *Phys. Rev. B* **79**, 024107 (2009).
 - ²⁷ M. P. Allen and D. J. Tildesley, *Computer Simulation of Liquids* (Oxford University Press, Oxford, 1989).
 - ²⁸ S. Chiesa, D. M. Ceperley, R. M. Martin, and M. Holzmann, *Phys. Rev. Lett.* **97**, 076404 (2006).
 - ²⁹ N. D. Drummond, R. J. Needs, A. Sorouri, and W. M. C. Foulkes, *Phys. Rev. B* **78**, 125106 (2008).
 - ³⁰ C. Lin, F. H. Zong, and D. M. Ceperley, *Phys. Rev. E* **64**, 016702 (2001).
 - ³¹ C. S. Yoo, B. Maddox, J.-H. P. Klepeis, V. Iota, W. Evans, A. McMahan, M. Y. Hu, P. Chow, M. Somayazulu, D. Hausermann, et al., *Phys. Rev. Lett.* **94**, 115502 (2005).
 - ³² L. Mitáš, E. L. Shirley, and D. M. Ceperley, *J. Chem. Phys.* **95**, 3467 (1991).
 - ³³ I. Ovcharenko, A. Aspuru-Guzik, and W. A. Lester, Jr., *J. Chem. Phys.* **114**, 7790 (2001).
 - ³⁴ Y. Lee, private communication, see also Y. Lee, P. R. C. Kent, M. D. Towler, R. J. Needs, and G. Rajagopal, *Phys. Rev. B* **62**, 13347 (2000) for large core version of these pseudopotentials.
 - ³⁵ L. K. Wagner, M. Bajdich, and L. Mitas, *J. Comput. Phys.* **228**, 3390 (2009), www.qwalk.org.
 - ³⁶ V. Saunders, R. Dovesi, C. Roetti, R. Orlando, C. M. Zicovich-Wilson, N. M. Harrison, K. Doll, B. Civalleri, I. Bush, P. D'Arco, et al., *CRYSTAL2003 User's Manual* (University of Torino, Torino, 2003).
 - ³⁷ P. Blaha, K. Schwarz, G. K. H. Madsen, D. Kvasnicka, and J. Luitz, *WIEN2k, An Augmented Plane Wave + Local Orbitals Program for Calculating Crystal Properties* (Techn. Universität Wien, Austria, 2001).
 - ³⁸ D. R. Linde, ed., *CRC Handbook of Chemistry and Physics* (CRC Press/Taylor and Francis, 2007).
 - ³⁹ J.-W. Lee, L. Mitas, and L. K. Wagner (2004), [arXiv:cond-mat/0411247](https://arxiv.org/abs/cond-mat/0411247).
 - ⁴⁰ L. Mitas and J. Kolorenč, *Rev. Mineral. Geochem.* **71**, xxx (2010).
 - ⁴¹ G. Ortiz, D. M. Ceperley, and R. M. Martin, *Phys. Rev. Lett.* **71**, 2777 (1993).
 - ⁴² J. Kolorenč and L. Mitas, *Phys. Rev. Lett.* **101**, 185502 (2008).
 - ⁴³ H. K. Bowen, D. Adler, and B. H. Auker, *J. Solid State Chem.* **12**, 355 (1975).
 - ⁴⁴ M. W. Schmidt, K. K. Baldrige, J. A. Boatz, S. T. Elbert, M. S. Gordon, J. H. Jensen, S. Koseki, N. Matsunaga, K. A. Nguyen, S. J. Su, et al., *J. Comput. Chem.* **14**, 1347 (1993).
 - ⁴⁵ M. Bajdich, L. Mitas, L. K. Wagner, and K. E. Schmidt, *Phys. Rev. B* **77**, 115112 (2008).
 - ⁴⁶ The 125 k points sample the whole Brillouin zone, they fold into 19 in the irreducible wedge of the Brillouin zone.